Pflugers Arch - Eur J Physiol (2004) 448: 248–258
DOI 10.1007/s00424-004-1246-9

INSTRUMENTS AND TECHNIQUES

Ezequiel Morales · Fernando R. Fernandez · Suzanne Sinclair · Michael L. Molineux · W. Hamish Mehaffey · Ray W. Turner

Releasing the peri-neuronal net to patch-clamp neurons in adult CNS

Received: 8 January 2004 / Accepted: 16 January 2004 / Published online: 17 February 2004

Abstract The extracellular matrix of adult neural tissue contains chondroitin sulphated proteogylcans that form a dense peri-neuronal net surrounding the cell body and proximal dendrites of many neuronal classes. Development of the peri-neuronal net beyond approximately postnatal day 17 obscures visualization and often access by patch electrodes to neuronal membranes with the result that patch clamp recordings are most readily obtained from early postnatal animals. We describe a technique in which the surface tension of a sucrose-based medium promotes partial dissociation of thin tissue slices from adult tissue. Surface tension spreads the tissue and loosens the peri-neuronal net from neuronal membranes within minutes and in the absence of proteolytic enzymes. Furthermore, the extent of dissociation can be controlled so as to maintain the overall slice structure and allow identification of specific cell classes. Excellent structural preservation of neurons and dendrites can be obtained and full access by patch electrodes made possible for current- or voltage-clamp recordings in tissue well beyond the development of peri-neuronal nets. We demonstrate the feasibility of using this approach through patch recordings from neurons in the brainstem and cerebellum of adult gymnotiform fish and in deep cerebellar nuclei of rats as old as 6 months.

Keywords Patch-clamp · Peri-neuronal net · Organotypic · Cell dissociation · Proteoglycan · Tissue print · Spread-printing · Deep cerebellar nucleus

*E. Morales and F. Fernandez contributed equally to this work

E. Morales · F. R. Fernandez · S. Sinclair · M. L. Molineux · W. H. Mehaffey · R. W. Turner (✉)
Neuroscience Research Group, University of Calgary,
3330 Hospital Dr. N.W.,
Calgary, Alberta, T2N 4N1, Canada
e-mail: rwturner@ucalgary.ca
Tel.: +1-403-2208452
Fax: +1-403-2832700

Introduction

Patch-clamp recording techniques have revolutionized electrophysiology by providing a high-quality seal between electrode and neuronal membrane and yet low-resistance access for voltage- and current-clamp analyses [18]. The use of differential interference contrast optics and infrared light transmission (DIC-IR) has, furthermore, allowed cells to be visualized and patch recording electrodes to be positioned with micron resolution [17]. As a result, patch recordings have been obtained from dendritic, axonal, and even presynaptic membranes in numerous brain regions [7, 15, 20, 59, 61]. In many areas, however, particularly the brain stem, patch clamp recordings are typically limited to early postnatal animals in the range of postnatal days (P)10–P17. After this age, visualization of cell processes under DIC-IR becomes much more difficult. A restriction to animals under P18 represents a serious limitation, in that the density and distribution of ion channels are often just approaching adult characteristics at ~P21 [4, 24, 42]. Although high-quality patch recordings have been obtained from older animals in vitro [39, 51], visibility is reduced under DIC-IR and the success rate for patching is far lower than in early postnatal animals.

Difficulties encountered in patch-clamping beyond ~P17 are generally considered to be due to an increased degree of myelination. However, an additional problem is the presence of a "peri-neuronal net" that forms a highly organized reticulum in the extracellular space and tightly surrounds the somatic and proximal dendritic regions of CNS neurons [14]. The complement of molecules that make up a peri-neuronal net varies between cell types, but generally comprises a family of lecticans complexed to hyaluronan and tenascin-R (for reviews see [14, 29, 66]). Peri-neuronal nets are essentially absent before ~P17 but then increase to adult levels beyond ~P21 [32, 33, 46, 47, 66]. The most heavily invested cell types are spinal motoneurons, deep cerebellar nuclear or vestibular neurons, cells of the auditory system, and parvalbumin-expressing cortical interneurons [6, 14, 32]. The function

of peri-neuronal nets is not fully known, although their appearance correlates with the development of adult neuronal characteristics [14, 30, 66].

A variety of dissociation and cell culture methodologies have been developed in the past which incidentally remove peri-neuronal nets; the most evident being mass dissociation for acute recordings or for establishing long-term cell cultures. However, mass dissociation results in significant disruption of neuronal structure, and obtaining viable cell cultures dictates that tissue be derived from embryonic or early postnatal animals. Acute dissociation can serve a similar purpose in removing peri-neuronal nets [31, 63], although enzymatic treatment and substantial tissue disruption is still required. Organotypic slice cultures provide a significant advantage in preserving slice and cell structure from later postnatal stages [22, 60]. However, organotypic cultures require extended time-frames for slice thinning that could potentially alter cell activity. In addition, peri-neuronal nets can still develop in organotypic or dissociated cultures along a time course similar to that in intact tissue [12, 38]. Tissue printing can extract neurons near the surface of a slice from adult tissue, but this method still works best if myelination and peri-neuronal net development is at an early stage [3, 28, 34].

The present report describes a modified tissue-print procedure termed "spread-printing" that allows thin tissue slices to partially dissociate within minutes in the absence of proteolytic enzymes. The resulting tissue retains an organotypic-like organization and often excellent neuronal somatic and dendritic morphology. We show that spread-printing effectively removes the peri-neuronal net from adult teleost brainstem neurons and rat cerebellar nuclear neurons up to at least 6 months of age, allowing patch recordings over the range of single channels to spike discharge.

Materials and methods

All chemicals were purchased from Sigma (St. Louis, Mo., USA) with the exceptions of iberiotoxin and tetrodotoxin (TTX, Alomone Labs; Israel), immunoreagents from Vector (Burlingame, Calif., USA), and fluorophores from Molecular Probes (Eugene, Ore., USA).

Preparation of brain tissue

All animal care and tissue dissection was carried out under the guidelines of the Canadian Council of Animal Care. Briefly, Brown Ghost Knife fish (*Apteronotus leptorhynchus*) of 6–24 months of age were obtained from importers and maintained in fresh-water aquaria at 26–28 °C. Fish were anaesthetized using 0.05% phenoxy-ethanol and the brain dissected out and mounted on a cutting block to prepare transverse tissue slices on a Vibratome according to established procedures [40]. Sprague Dawley rats were purchased as pregnant dams with pups (Charles River, Montreal, Canada) and maintained in the animal care facility. Male pups P15–P32 or dams up to 6 months old were anaesthetized with sodium phenobarbital (65 mg/kg) followed by a transcardial perfusion with ice-cold artificial cerebrospinal fluid (aCSF) containing (in mM): NaCl 125, KCl 3.25, $CaCl_2$ 1.5, $MgCl_2$ 1.5, $NaHCO_3$ 25 and D-glucose 25 continuously oxygenated with 95% O_2 and 5% CO_2. Following decapitation the hindbrain was removed and the cerebellum separated and blocked in the presence of ice-cold aCSF to cut coronal or sagittal cerebellar sections by vibratome. After preparing spread prints (see below), cerebellar tissue was incubated for 30 min at 34 °C and then maintained at room temperature prior to recordings in oxygenated aCSF.

Gelatine Bloom 275 (Fisher Scientific, Fair Lawn N.J., USA) was made up as a 20% solution in distilled water by applying moderate heat while mixing before loading into a series of 3-ml syringes. The syringes were cooled by standing upright to allow trapped gas to rise to the top and dissipate, and then stored at 4 °C for up to 3 weeks. Just prior to dissection a gelatine-containing syringe was warmed for 2–3 min in a beaker of hot tap water to allow ejection over and around the blocked brain. This encased the brain and provided support during cutting.

Spread-print slices were maintained as a submerged preparation on the stage of a Zeiss Axioskop 2 or Olympus B51-WI microscope and perfused with oxygenated aCSF comprising (in mM): 124 NaCl, 2.0 KCl, 1.25 KH_2PO_4, 1.5 $CaCl_2$, 1.5 $MgSO_4$, 24 $NaHCO_3$ and 25 D-glucose, pH 7.4. Electrosensory lateral line lobe (ELL) slices were maintained at room temperature and rat tissue at 34 °C.

Patch recordings

Cells were visualized for patch recordings using DIC-IR with a Newvicon camera (Dage MTI) or Hamamatsu C24000 and video monitors (Hitachi VM9012U). Drugs were added to the bath. Patch electrodes were produced on a Sutter P-87 microelectrode puller from borosilicate glass (fibre-filled 1.5 mm O.D.; A-M Systems, Carlsborg, Wash., USA), fire-polished and the tips silicon-coated (Sylgard 184) under microscopic observation. Recordings were obtained using Axoclamp 2A, Axopatch 200-A or 700A amplifiers, digitized (Pclamp 8.0 software, Axon Instruments, Union City, Calif., USA) and stored for off-line analysis (Igor Pro, Lake Oswega, Minn., USA; Corel Draw, Ottawa, Canada; Adobe Illustrator 9.0, San Jose, Calif., USA).

The pipette solution for whole-cell teleost recordings was (in mM) KCl 144, HEPES 5, $MgCl_2$ 1, EGTA 5, Mg-ATP 1.5, 0.1 $CaCl_2$, pH 7.2. Mammalian whole-cell recordings used (in mM): K-methyl-SO_4 130, EGTA 0.1, HEPES 10, NaCl 7, $MgCl_2$ 0.3, di-tris-creatine PO_4 5, tris-ATP 2 and Na^+-GTP 0.5, pH 7.3. Electrode resistance was typically 2–5 MΩ and the series resistance of 5–15 MΩ was corrected by compensation at 80–90%. Seals were 1.5 GΩ or greater and any leak currents were subtracted on-line. All ELL voltage-clamp recordings were made in the presence of 1 µM TTX and in some cases 200 µM Cd^{2+} and 0.1 mM $CaCl_2$ in which $MgCl_2$ and KCl were substituted for $MgSO_4$ and KH_2PO_4, respectively. Voltage-clamp whole-cell recordings were obtained at 2–5 kHz and single-channel recordings in the on-cell or outside-out configuration at 5 kHz. Current-clamp recordings were obtained at 10 kHz.

Tissue preparation for immunocytochemistry

After cutting on the vibratome, spread or unspread tissue slices were mounted on cover-slips and fixed overnight in 4% paraformaldehyde in 0.1 M phosphate-buffered saline (PBS) at 4 °C. After 3×20 min washes the tissue was treated in a working solution containing 0.1% Triton-X 100 and 3% normal horse serum in PBS for 1 h and then overnight at 4 °C in biotinylated *Wisteria floribunda* lectin (WFA; 20 µg/ml) or, in some cases, mouse anti-tubulin (1:200; gift of M. Klymkowsky, University of Colorado, Colo., USA). Sections were then washed 3×20 min in working solution, exposed to streptavidin-Cy3 (1:1,500) and/or donkey anti-mouse AlexaFluor 488 (1:500) for 2 h at room temperature, washed in PBS and mounted on a microscope slide in anti-fade medium. Fluorescent labelling was imaged on an Olympus FV300 BX50 confocal

microscope with FluoView software and images transferred to Adobe Photoshop 6.0 and Adobe Illustrator 9.0 for figure preparation.

Tissue preparation for scanning electron microscopy (SEM)

Spread-printed slices were fixed by immersion in 4% paraformaldehyde in 0.1 M PBS and postfixed overnight at 4 °C. The tissue was dehydrated in increasing concentrations of ethanol (30%, 50%, 75%, 100%) for 15-min periods, 100% ethanol for 1 hr and then overnight at 4 °C. Tissue samples were critical point dried at 1,100 psi and 32 °C. Cover-slips containing the tissue samples were mounted on 12-mm SEM pins using double-sided tape, then coated with gold. Samples were imaged using scanning electron microscopes (Hitachi 20 kV; Phillips/FEI ESEM 20 kV) and negatives subsequently scanned for image processing (Nikon 2000). All images were processed in Adobe Photoshop 6.0 and Illustrator 9.0.

Results

Patch recording in adult teleost brainstem

The electrosensory lateral line lobe (ELL) is a primary sensory nucleus in the medulla of apteronotid fish. The ELL receives primary afferent input from electroreceptors that encode electric field distortions in the surrounding environment to localize sensory inputs [5]. ELL pyramidal cells form a distinct cell body layer and project large diameter apical dendrites into an overlying molecular layer. The activity of pyramidal cells has been studied extensively through microelectrode recordings in vivo and in vitro, with recent work describing burst discharge involved in processing sensory inputs [21, 36, 40, 50].

Applying patch-clamp technology to understand soma-dendritic interactions in burst discharge has been slowed, however, by the presence of a dense layer of material in the cell body region. Thus, even under DIC-IR optics the pyramidal cell body layer appears to be covered with a dense conglomerate of opaque, lipid-like spheres of 2–5 µm diameter that completely prevents visualization of cell bodies or their approach by patch electrodes. Given difficulties in obtaining very young apertonotids from suppliers, we originally attributed this barrier to the presence of myelinated fibres in adult tissue. However, a growing body of evidence indicates the presence of a peri-neuronal net around adult CNS neurons that helps account for difficulties in patch-clamping adult cells.

A host of lectins and antibodies have been used to reveal different molecular components of peri-neuronal nets [14]. To localize peri-neuronal nets we used biotinylated WFA, a lectin that binds to *N*-acetylgalactosamine, a common component in peri-neuronal nets. Application of biotinylated WFA to fixed tissue revealed a dense distribution of WFA binding sites primarily in the pyramidal cell body layer (Fig. 1A,B). Substantially less label was detected in the overlying molecular layer and underlying plexiform layer that contains pyramidal cell axons. Higher magnification indicated that the fluorescent label was tightly associated with the external surface of pyramidal cell body membranes and over the initial 50 µm of apical or basilar dendritic shafts (Fig. 1C, D). This distribution of label is typical of that found for peri-neuronal nets around numerous cell types in adult CNS [6, 14].

Spread-print preparation

To gain further access to somatic membranes, we modified a tissue-print procedure to obtain "spread-prints" of tissue slices. With this approach the surface tension of a solution is used to apply tension over the entire circumference of a thin tissue slice. Tissue was prepared by cutting on a vibratome using standard procedures of blocking and mounting the brain on a cutting block with cyanoacrylate glue. Before filling the vibratome chamber with medium, the brain was surrounded with a warmed solution of gelatine. Subsequent addition of cold aCSF solidified the gelatine to a consistency firm enough to enable consistent cutting of 80–120 µm slices. Tissue slices were cut in ice-cold, oxygenated (95% O_2/5% CO_2) aCSF, or in a "print medium" consisting of a modified sucrose-based aCSF (in mM): sucrose 218, $NaHCO_3$ 25, K-gluconate 3.25, $MgCl_2$ 4.5, $CaCl_2$ 0.1, D-glucose 10, Na-pyruvate 1, pH 7.4. This medium is a combination of that often used to cut tissue

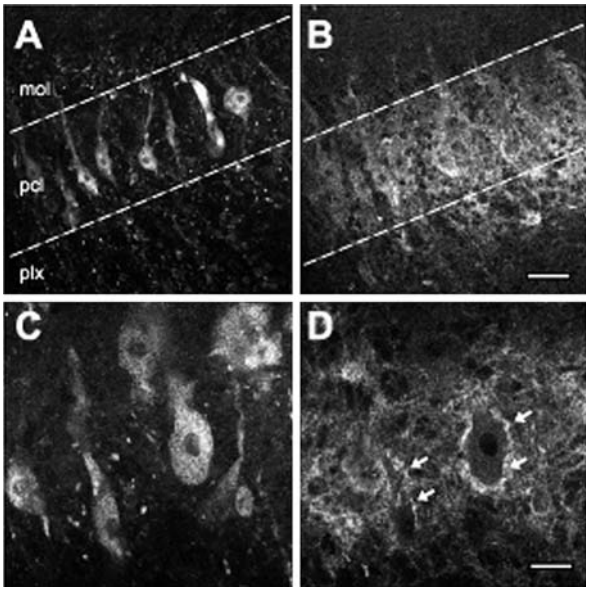

Fig. 1A–D A peri-neuronal net surrounds neurons in adult teleost medulla. The presence of *N*-acetylgalactosamine was revealed through binding of biotinylated *Wisteria floribunda* (WFA) lectin and streptavidin-Cy3. **A**, **B** A low-power image of the electrosensory lateral line lobe (ELL) pyramidal cell layer as visualized by immunolabels for tubulin (**A**) and binding sites for WFA (**B**). Note the restriction of the peri-neuronal net matrix to the cell body layer and proximal dendritic aspects of cells within the pyramidal cell body layer (*pcl*). No labelling is evident in the overlying molecular layer (*mol*) or underlying plexiform layer (*plx*). **C**, **D** A higher-magnification image of the label for tubulin (**C**) reveals the pyramidal cell bodies and proximal dendrites; Cy3 labelling (**D**) shows the dense peri-neuronal matrix that surrounds the cell body region (*arrows*). *Scale bars*: **A**, **B** 50 µm; **C**, **D** 20 µm

slices in the presence of equimolar sucrose and a low Ca^{2+}/high Mg^{2+} concentration to prepare tissue for dissociation [2, 34, 35]. Replacing KCl with K-gluconate significantly improved cell structure. After cutting slices of 80–120 µm thickness, the tissue was lifted from the chamber with a flat spatula and 000 brush and coaxed onto the surface of cold and pre-oxygenated print medium contained within a 35-mm Petri dish. The cover was then replaced to maintain humidity and the partial pressure of gases. We found it very important to ensure that the print medium used to fill the Petri dish be as cold as possible, with the result that slices would essentially "jump" from the spatula onto the medium surface. If not ice-cold, slices often fell below the medium surface and the spreading process would not take place. Approximately 2 ml cold print medium in a 35-mm Petri dish had sufficient surface tension to apply a gentle but consistent centrifugal tension around the entire slice. As a result, the ELL pyramidal cell body layer began to dissociate partly within 2–10 min, while relatively little effect could be detected visually in the region of the molecular layer (Fig. 2A, B).

When viewed under a dissecting microscope, the spreading process comprised not so much a tearing or stretching of neuronal tissue as a slow "unknitting" of cell processes as the extracellular matrix holding cells together gradually loosened. If soma and dendrites did separate, it usually took the form of a clean break with subsequent sealing of the cut surface. When the tissue had dissociated to the desired extent it was transferred to a dry glass cover-slip coated previously with gelatine (20%) by attaching the cover-slip to a bent spatula tip using a rolled piece of tape. By lowering the cover-slip parallel to the slice surface and then pressing down to partially submerge cover-slip and slice, the slice attached to the cover-slip and the dissociation process stopped immediately. The cover-slip was then removed from the tape by forceps and the cover-slip stored in 35-mm Petri dishes containing aCSF for later use.

Slices were maintained for subsequent recording by placing the cover-slips in an oxygenated holding chamber at room temperature, while mammalian tissue was subjected to an additional 30 min incubation at 34 °C prior to storage at room temperature. Teleost brainstem slices could also be cut and spread in a HEPES-based print medium and then stored very successfully for many hours at 4 °C.

The time required to achieve visible dissociation varied according to the tissue used and with the orientation of the cut (sagittal or transverse), a result probably reflecting the different orientation of axon fibre tracts holding the tissue together. In support of this, we found that while the ELL pyramidal cell body layer dissociated within minutes, the molecular layer rarely dissociated, presumably due to the dense and interwoven cerebellar parallel fibres that project onto pyramidal cell dendrites [44]. Similarly, dissociation of the cell body layer could be achieved within just a few minutes in transverse slices, but little if any dissociation was obtained when slices were cut with a longitudinal orientation. Rat deep cerebellar nuclei required similar times for spreading, while preliminary work on hypothalamic slices suggests that more than 30 min is required. The tension provided during the spreading process could

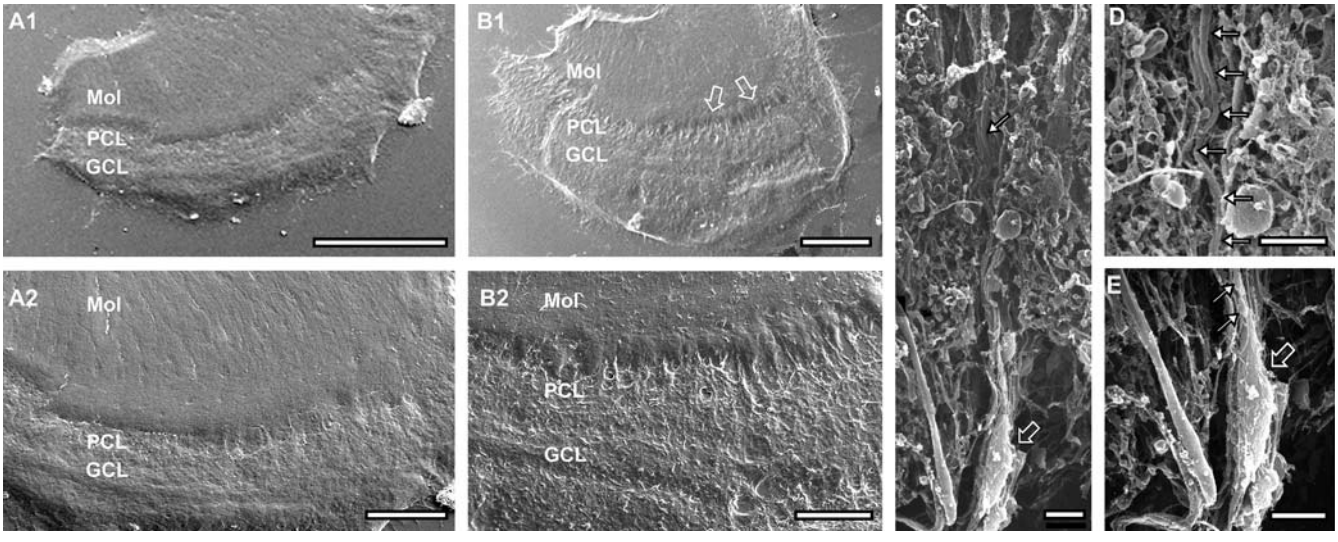

Fig. 2A–E Spread-printing achieves partial dissociation of tissue slices and maintains an organotypic organization. **A**, **B** Scanning electron micrographs of an intact ELL tissue slice (**A***1*, **A***2*) and a second slice partially dissociated through spread-printing (**B***1*, **B***2*). The position of the pyramidal cell layer (*PCL*), molecular layer (*Mol*), and granule cell layer (*GCL*) are indicated. Note the partial dissociation of the PCL and GCL in the lateral aspect of the ELL (**B***1*; *arrows*) but relatively little effect on the remaining extent of the ELL, thus preserving an organotypic organization. Higher magnification of the PCL and GCL in **A***2* and **B***2* at the same scale indicates how spread printing expands the cell body layers, greatly improving visualization of cellular structures. **C**–**E** Higher-magnification scanning electron micrographs of a single pyramidal cell and apical dendritic extensions in a spread-printed slice. A low-power image (**C**) indicates the ability to track continuous segments of dendrites and soma, while higher magnification shows a set of dendritic branches (**D**, *arrows*) and the soma (**E**, *open arrow*). Note the additional ability to resolve individual, large-diameter GABAergic synaptic boutons (**E**, *arrows*). *Scale bars*: **A***1*, **B***1* 500 µm; **A***2*, **B***2* 200 µm; **C**, **D** 5 µm

be adjusted by raising or lowering the volume of medium, with a lower volume increasing surface tension and the rate of tissue spreading. We also adjusted the thickness of slices to accommodate subtle differences in axonal orientation during vibratome cutting, decreasing slice thickness to promote greater dissociation.

Several enzymes have been identified that can break down different components of peri-neuronal nets when injected in vivo or when applied to fixed tissue for extended periods of time [10, 12, 33, 46]. We tested the ability of chondroitinase ABC (0.2 units/ml), collagenase (5 units/ml) and *N*-acetylgalactosaminase (2 units/ml) to improve the spread-print process by applying enzymes

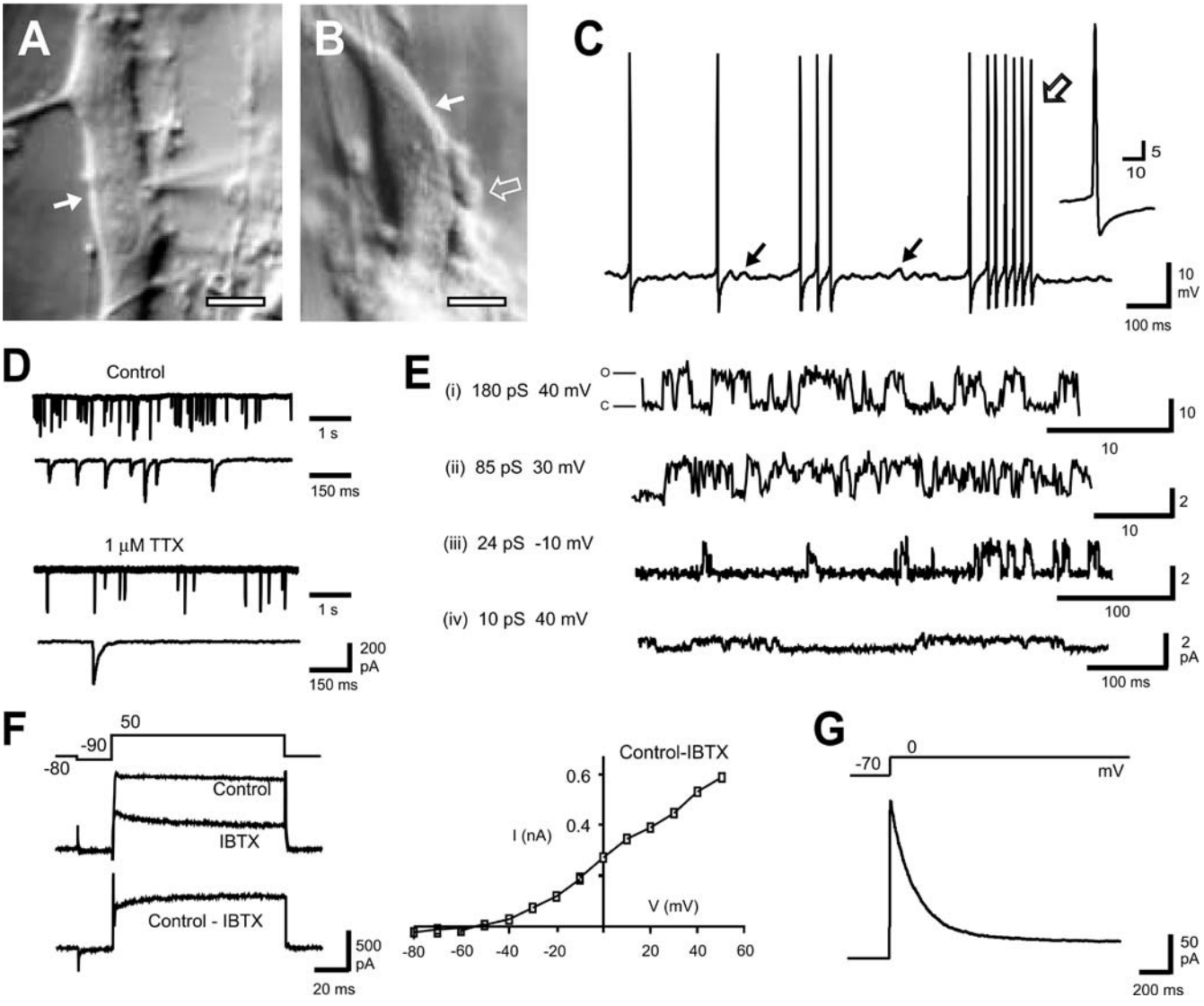

Fig. 3A–G Patch-clamp recordings of ELL pyramidal cells in spread-printed slices. **A**, **B** Differential interference contrast optics and infrared light transmission (DIC-IR) images of ELL pyramidal cells exposed for patch clamp recordings through spread-printing. Note the high contrast and clean surface of membranes (*solid arrows*) and proximal dendritic trunks. A small cluster of glia and peri-neuronal matrix that was not removed is shown by an *open arrow* in **B**. **C** Spontaneous Na^+ spike discharge in a whole-cell recording from a pyramidal cell illustrating large amplitude and narrow duration spikes with prominent hyperpolarizing after-potentials (AHPs, *inset* shows a single spike expanded). A burst of spikes near the end of the record (*open arrow*) is indicative of a burst mechanism in pyramidal cells that depends on an intact dendritic arborization. *Arrows* denote putative spontaneous synaptic depolarizations. **D** Spontaneous synaptic currents recorded in whole-cell voltage clamp with 140 mM KCl in the patch pipette (long and short time bases are shown). Bath application of 1 μM tetrodotoxin (*TTX*) greatly reduces the frequency of spontaneous activity (*lower traces*). **E** Single-channel recordings from ELL pyramidal cell somata in spread-printed slices showing four classes of K^+ channels. The calculated single-channel conductance and pipette holding potential for the traces are indicated to the *left*. Recordings *i*, *ii* and *iv* were made in the on-cell mode under conditions of symmetric [K^+] and in *iii* in the outside-out configuration with 140 mM KCl. All channel activity was recorded at 5 kHz and digitally filtered (in *i* and *ii* at 2 kHz, in *iii* at 700 Hz and in *iv* at 150 Hz). **F** Whole-cell voltage clamp recording from a pyramidal cell in a spread-printed slice at the indicated step potentials before and after application of 200 nM iberiotoxin (*IBTX*). Iberiotoxin-sensitive currents are shown in the *lower trace* with the associated current/voltage (*I*/*V*) plot on the *right*. **G** An outside-out macropatch recording pulled from the soma of a pyramidal cell showing Kv3 K^+ currents. *Scale bars*: **A**, **B** 10 μm

during the cutting and spreading procedure. However, we noticed little effect on the degree of dissociation over the short times used here. It is also expected that the activity of these enzymes was marginal at the low temperatures required during the spreading process. Although pre-incubating slices in enzymes at higher temperatures may well improve the extent of dissociation, the tendency for slices to become "sticky" after enzyme treatment may complicate their transfer to the surface of print medium for spreading. The high cost of these enzymes is also prohibitive for daily slice preparation.

Structure and physiology of teleost brainstem and cerebellar spread-prints

One of the key advantages of spread-printing is that the extent of dissociation can be visualized directly and then stopped at any point by attaching the slice to a cover-slip. Because dissociation begins with a normal tissue slice, spread-printing can preserve the major landmarks of the slice (Fig. 2A, B). Although we expect some aspects of glial or network structure to be disrupted, we use the term "organotypic" to describe a slice in which specific cell types can be identified in different regions of a slice. Structural preservation of cells and processes is also far superior to that obtained with mass dissociation. Finally, the entire process is fast and without the influence of proteolytic enzymes on ion channel activities. One can thus proceed from blocked brain to an organotypic slice attached firmly to a cover-slip and onto the stage of a microscope within 15 min. Each of these factors provides a tremendous advantage in identifying specific regions and individual cell classes for recording. In the case of the ELL, it allows one to target a basilar vs. non-basilar pyramidal cell class or cells from within one of four topographic maps that can be distinguished across the medio-lateral axis [5, 43]. In rat cerebellum one can focus on recording from large vs. small neurons in only one of the deep cerebellar nuclei.

Imaging at the cellular level through SEM or DIC revealed that spread-printing effectively loosened the extracellular matrix, improving visualization of neuronal structures and access by patch-recording electrodes. In the ELL pyramidal cell body layer spread-printing removed an ordinarily dense complex of glia cells and extracellular matrix, leaving variable segments of membrane free for approach by patch electrodes (Figs. 2C–E and 3A, B). Although there was substantially less dissociation of tissue in the molecular layer, spread-printing cleared elements of the extracellular matrix near the slice surface, again improving access to dendritic membranes (Fig. 2C, D). As found for any dissociation process, cell health varied according to the degree of dissociation and local conditions. We also found that smaller diameter neurons were most readily exposed with this approach, while larger cells (i.e. cerebellar Purkinje cells) were less able to accommodate the tensions generated during spread-printing.

Most ELL pyramidal cell recordings were obtained from slices in which a minimal degree of dissociation allowed visualization of as little as 2 μm^2 of somatic membrane and thus attachment of patch electrodes. If the spreading process was left longer, the inherent structure of the ELL promoted a much more extensive dissociation in the form of a progressive "unzippering" of the cell line. This differed in other structures (i.e. hypothalamus, cerebellar cortex, granule cell layer or deep nuclei) where we noted a more distributed rate of dissociation, such that the tissue underwent a more gradual and less extensive disruption. However, even in extensively dissociated ELL we found several pyramidal cell somata with good structural preservation per slice in which glia and the peri-neuronal matrix was removed (Fig. 3A, B).

Current-clamp recordings in ELL pyramidal cells using patch electrodes registered average resting membrane potentials of −61.3±1.6 mV and input resistances of 374 ±60 MΩ (n=6). In all cells we detected large-amplitude, narrow-duration Na^+ spikes discharging spontaneously (Fig. 3C) or in response to direct current injection (not shown). In some cases we could detect burst discharge that included the generation of a progressively larger depolarizing after-potential and termination of the burst by a spike doublet (Fig. 3C). This burst process has been examined carefully and depends on a conditional back-propagation of dendritic spikes [40, 50]. The presence of this form of burst discharge thus indicates the ability to preserve coordinated activity between somatic and dendritic regions.

A certain number of synaptic contacts could also be preserved in spread-prints; seen directly as large-diameter synaptic boutons on pyramidal cell somata under SEM (Fig. 2E, arrows) or as spontaneous synaptic depolarizations in pyramidal cell recordings (Fig. 3C). Spontaneous postsynaptic currents (PSCs) could be recorded in the whole-cell, voltage-clamp mode in pyramidal cell somata as a series of inwards currents comprising both IPSCs and EPSCs under conditions of high KCl in the patch pipette (Fig. 3D). The frequency of PSCs could be reduced by bath application of TTX, suggesting that these responses comprised both miniature synaptic currents and transmitter release dependent on spike discharge in the presynaptic axon (Fig. 3D). A form of slow spontaneous burst discharge that arises from synaptic interactions between pyramidal cells and an underlying layer of granule cells was also found in some slices (data not shown) [64]. However, the variable extent of dissociation inherent to spread-printing ELL slices made it difficult to predict the degree to which sufficient circuitry could be retained to support stimulus-evoked synaptic responses. Preliminary tests on stimulating the tractus stratum fibrosum input to ELL pyramidal cell proximal dendrites were unsuccessful, although we did not pursue this in great detail. It is expected that the ability to evoke synaptic responses will depend on how a given slice dissociates, a property that will need to be determined for each preparation.

High quality gigaohm seals could be formed on spread-printed cells, with the ability to record at least four

conductance levels of K^+ channels (Fig. 3E). These included large-conductance channels of 120–200 pS (Fig. 3E, i), intermediate-conductance channels of 70–90 pS (Fig. 3E, ii), Kv3 K^+ channels of ~24 pS (Fig. 3E, iii) [19, 54] and lower-conductance K^+ channels of 5–15 pS (Fig. 3E, iv). In some cases, a clear separation and sealing at a breakpoint between soma and dendrites was obtained, providing the interesting possibility of applying whole-cell voltage clamp analysis with minimal predicted problems due to space-clamp errors. Figure 3*F* shows a cell in which whole-cell voltage clamp was applied to distinguish the iberiotoxin-sensitive component of whole-cell current and its associated current/voltage (*I*/*V*) relationship. Outside-out recordings could be made readily from pyramidal cell somata or apical dendrites of spread-printed slices (Fig. 3G) [54].

Spread-printing appeared to produce little visible dissociation of the overlying cerebellar lobules; the corpus cerebelli (CCb) or the eminentia granularis pars posterior (EGp) [56]. SEM imaging of the EGp granule cell layer indicated that normal tissue was composed of tightly packed, small-diameter granule cells (Fig. 4A). Spread-printing increased the separation between granule cells presumably by disrupting the extracellular matrix, allowing visualization of granule cell axons and parallel fibre bundles progressing towards the molecular layer (Fig. 4B, C). Whole-cell voltage clamp of EGp granule cells in spread-printed slices revealed both fast inward Na^+ and substantial outward K^+ currents (Fig. 4D), indicating the viability of cells after the spreading process.

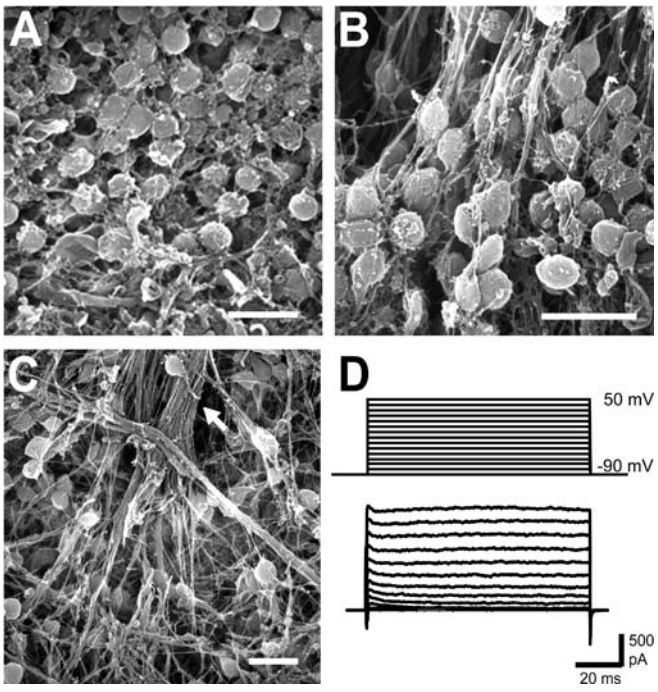

Fig. 4A–D Spread-printing improves access to cerebellar granule cells. **A** Scanning electron micrograph of the typical dense packing of granule cells in the eminentia granularis pars posterior (EGp) lobe of apteronotid cerebellum in untreated tissue. **B** A scanning electron micrograph of EGp granule cells after spread-printing illustrates the improved resolution of individual cells and parallel fibre axons coursing towards the molecular layer. **C** A lower-power micrograph indicating the resolution of bundles of granule cell parallel fibres (*arrow*) as they coalesce before projecting to the molecular layer in a spread-printed slice. Note how the spreading process can improve access to both electrodes and immunoreagents by expanding the extracellular space. **D** Whole-cell patch recording of an EGp granule cell from a spread-print slice preparation reveals both inward and outward currents in the presence of normal artificial cerebrospinal fluid (aCSF). Step commands were given from a holding potential of −90 mV in 10-mV steps to 50 mV. *Scale bars*: **A**–**C** 5 μm

Mammalian cerebellar nuclei

One region of the mammalian CNS noted for both an early development and dense expression of extracellular proteoglycans is the cerebellar nuclei [6, 37]. The appearance of peri-neuronal nets in this structure at ~P17 has also slowed the application of patch clamp technology due to difficulties in distinguishing cell somata or dendrites. The only way in which this barrier has been overcome to date has been to employ mass dissociation or to restrict recordings to ages below ~P18 [1, 23, 52]. We thus tested the spread-print approach as a means of gaining access to deep nuclear cells for patch clamp recording. Despite the dense structure and heavy investment of axonal projections, spread-printing cerebellar nuclei required no more time than for teleost brainstem, even though less dissociation was apparent upon visual inspection. The key factor was cutting slices less than 150 μm thickness (usually 100 μm).

Reacting cerebellar nuclei for WFA binding sites revealed that in normal, unspread tissue, cell bodies and dendrites were obscured by an overlying haze of proteoglycans, as revealed with streptavidin-Cy3 (Fig. 5A). Spread-printing removed this overlying material and provided a much better image of cell bodies and proximal dendrites of nuclear neurons (Fig. 5B). The degree to which cells were masked in normal tissue can be appreciated under DIC-IR optics (Fig. 5C), with spread-printing substantially improving the imaging of somata and proximal dendrites (Fig. 5D). Although some membrane-associated WFA binding sites could still be detected after spread-printing (Fig. 5B), we consistently gained better access to healthy neurons and increased the success rate of obtaining whole-cell recordings. This was the case for all ages tested, with recordings obtained from rats as old as 6 months (Fig. 5E).

Current-clamp recordings revealed spontaneous Na^+ spike discharge of 5–50 Hz at resting membrane potentials of −50.7±0.9 mV and input resistances of 432±100 MΩ (n=5). Rebound depolarizations (RD) could be evoked following a step membrane hyperpolarization, indicating the preservation of the Na^+, hyperpolarization-activated cation (I_h), K^+ and Ca^{2+} currents believed responsible for this activity in normal tissue (Fig. 5E) [1, 16, 52]. Na^+ spike frequency also correlated closely with the magnitude of a preceding step hyperpolarization (Fig. 5E), as expected for healthy cerebellar nuclear neurons [1, 16, 52]. Finally, single-channel recordings could be performed

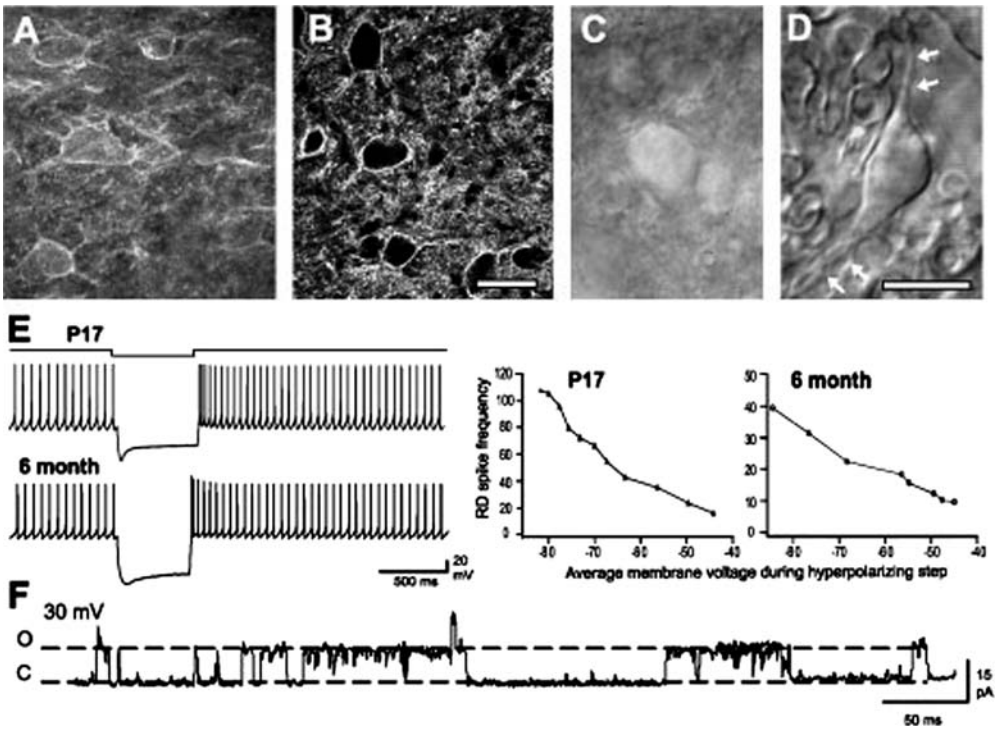

Fig. 5A–F Spread-printing improves patch electrode access in rat cerebellar nuclei. **A**, **B** Fluorescent labelling of nuclear cells in normal (**A**) and spread-printed (**B**) tissue slices from the same postnatal day (P)24 animal using biotinylated WFA-Cy3 to reveal peri-neuronal nets. In normal tissue (**A**) a diffuse fluorescent label obscures visualization of underlying cells that are surrounded by additional membrane-associated WFA binding sites. After spread-printing (**B**), individual cells are more easily visualized despite residual membrane-associated WFA binding sites. **C**, **D** DIC-IR images of nuclear cells at P17 in untreated tissue (**C**) and in another slice after spread-printing (**D**). Note the improved resolution of cell bodies and dendrites (**D**, *arrows*) after spread-printing. **E** Spontaneous spike discharge and a hyperpolarization-induced rebound depolarization in deep nuclear cells in a spread-print preparation from P17 and 6-month animals. Step hyperpolarization evoked by a −0.28-nA pulse for the P17 and a −0.1-nA pulse for the 6 month preparations. *Right*: plots of instantaneous spike frequency for the first two spikes of a hyperpolarization-induced rebound depolarization against membrane voltage attained during the step hyperpolarization. **F** An on-cell patch recording of large-conductance (presumed BK) K^+ channels from the soma of a spread-printed neuron from P17. A pipette potential of 30 mV is shown at *left*, open (*O*) and closed (*C*) states are indicated by *dashed lines*. *Scale bars*: **A**, **B** 50 μm; **C**, **D** 20 μm

in either on-cell or outside-out configuration in spread-printed slices (Fig. 5F).

Discussion

The present report describes a fast and effective means for partial dissociation of brain slices to loosen the dense peri-neuronal net from neuronal membranes. Excellent preservation of cell structure can be obtained, allowing identification of specific cell classes according to morphology and spatial information. As a result, patch-clamp recordings can be obtained from neurons that are normally inaccessible, extending patch recordings from early postnatal to adult animals.

Peri-neuronal nets were first described in the 1800s as an intricate reticulum that surrounds neuronal cell bodies and proximal dendrites [14]. It is now recognized that the peri-neuronal net is part of the extracellular matrix and that both neurons and glia contribute to producing the constituent molecular components [38, 46, 62]. Different compounds of the net are produced with distinct developmental time courses, but the net increases in complexity towards adult levels by ~P21 [32, 47]. The peri-neuronal net is made up of a family of chondroitin-sulphated proteoglycans that provide attachment sites for ligands such as tenascin-R and hyaluronan [66]. The nets are more prevalent in brainstem regions and are heavily associated with spinal motoneurons, cerebellar and vestibular neurons, auditory neurons and parvalbumin-containing interneurons in cortical regions [6, 11, 13, 27, 32, 41, 48]. There is evidence that peri-neuronal nets act to restrict plasticity in synapse formation and to guide dendritic morphology during development [62, 66]. The prevalence of peri-neuronal nets around cells that express high-threshold Kv3.1 K^+ channels or that generate high frequencies of spike discharge has led to suggestions that nets form a high anionic environment that promotes high-frequency output [9, 26].

From a practical point of view, peri-neuronal nets can present a significant barrier to visualization of neurons under DIC-IR optics in vitro and thus the ability to target specific structures with patch electrodes. One might expect to be able to remove some components of the net by applying enzymes directed against specific molecular elements, as has been achieved in vivo and in fixed tissue

[10, 33, 49]. Our attempts to use enzymes to help remove the peri-neuronal net were unsuccessful at the temperature and times required for spread-printing, and were too costly to prepare slices on a daily basis.

Several other dissociation techniques can improve patch electrode access, each with their own advantages and disadvantages [2, 3, 22, 25, 31, 34, 60, 63, 65]. Of the dissociation techniques currently available, spread-printing is most similar to a gradual dissociation of cell layers obtained through vibration or shaking [25]. However, this latter approach differs in requiring proteolytic enzyme treatment or substantial vibration to loosen cells, while spread-printing proceeds without need for mechanical treatment. Non-dissociative techniques can also be used to increase the visibility of cells for patch clamping. A "cleaning" approach can be used for some cells [18], but it proved to be unsuccessful for the brainstem neurons studied here. Although "blind-patching" techniques can be used (particularly in vivo [45, 55]), visualization of cells in vitro can greatly extend patch recordings to finer structures [7, 15, 20, 59, 61]. By improving visualization of cells in difficult tissues spread-printing can increase the success of patch recording in comparison to blind-patching.

Strengths and weaknesses

Spread-printing improves access for patch recordings by combining several of the advantages inherent to different dissociation methods. The strengths of spread-printing include (i) the short time required for dissociation, (ii) lack of proteolytic enzymes, (iii) careful control over the degree and time of dissociation, (iv) an organotypic organization of the dissociated preparation, (v) very high yield of identifiable neurons compared with other dissociation techniques, (vi) excellent morphology of isolated somata and dendrites and (vii) preservation of ion channel activities including Na^+, I_h, Ca^{2+}, and voltage- and Ca^{2+}-activated K^+ channels. Altogether these factors permit a wide range of patch recordings, from single channels to coordinated spike output from adult CNS, within minutes of cutting on a vibratome. Notably, the increased distance between cells in even mildly spread tissue also increases the penetration of immunoreagents below the slice surface, as confirmed in immunocytochemical studies [53]. It will be interesting to determine how spread printing can improve access to other preparations such as retina or even muscle preparations.

Potential drawbacks of the technique are similar to those of other dissociation methods in terms of the need to restrict recordings to cells not adversely affected by the dissociation process. In general we found that the smaller-diameter neurons were most resilient to the spreading process. It is unknown to what extent this might be due to the generally recognized difficulty of maintaining large diameter cells from older animals in a healthy state during slice preparation. Although spread-printing is not expected to overcome this problem, it at least removes the physical barriers present in older tissue and increases the probability of locating healthy neurons. In our case this translated to recordings from large cells of rat cerebellar nuclei up to 6 months of age, and teleost brainstem up to 2 years. Spread-prints must also be prepared from relatively thin slices to allow the print medium to exert sufficient force to loosen the peri-neuronal net. Although we could visualize apparently intact synaptic inputs through SEM and record spontaneous synaptic events, a thinner slice will undoubtedly lose some number of synaptic projections or circuit elements, particularly in regions of maximum spread. It should be noted that areas that are more resistant to spreading, such as the ELL molecular layer, are likely to retain intact synapses. However, in spread regions, the total conductance of an evoked synaptic input may be underestimated. Further caution should be taken in interpreting the kinetics and dynamics of synaptic responses, since disruption of the glial network potentially could increase response duration by reducing transmitter uptake. Adjacent glia can also alter release probability [8] which could modulate activity in an intact slice. These problems are of course inherent to all dissociated cell preparations, with additional potential difficulties associated with blocking glial proliferation in dissociated [57] and slice cultures [58]. We thus expect that a minimally spread slice reflects a situation intermediate between the organotypic connectivity found in slice cultures and the complete removal of network elements by dissociation.

Finally, there is potential for spread-printing to increase the activity of stretch-activated ion channels. We have no specific evidence at this time to refute or support this possibility. Given that many cells had normal resting membrane potentials and spike activity, stretch-activated channels would not appear to be a major concern. In addition, one can spread a slice as little as possible to gain electrode access under DIC-IR through openings in the extracellular matrix that span only a few square microns.

In summary, spread-printing can provide rapid access to neuronal membranes for either patch recording or immunocytochemical purposes. We demonstrate the potential to apply this technique in mammalian and teleost tissues well past the age of development for peri-neuronal nets. Although spread-printing has been attempted on only a few preparations to date, our preliminary work on cerebellar and deep cerebellar neurons indicates that this approach will be widely applicable to many other nuclei.

Acknowledgements We gratefully acknowledge the expert technical assistance of M. Kruskic, R. Humphreys for assistance with scanning EM, B.E. McKay for preliminary work on cerebellar cortex, and P. Whelan for use of a recording system. This work was supported by CIHR grants and an AHFMR Scientist award to RWT.

References

1. Aizenman, CD, Linden DJ (1999) Regulation of the rebound depolarization and spontaneous firing patterns of deep nuclear neurons in slices of rat cerebellum. J Neurophysiol 82:1697–1709

2. Baker, GB, Boulton AA, Walz W (eds) (1992) Practical cell culture techniques (Neuromethods series, Vol. 23). Humana Press, Totowa, pp xix, 392
3. Barres BA, Koroshetz WJ, Chun LL, Corey DP (1990) Ion channel expression by white matter glia: the type-1 astrocyte. Neuron 5:527–544
4. Beckh S, Noda M, Lubbert H, Numa S (1989) Differential regulation of three sodium channel messenger RNAs in the rat central nervous system during development. EMBO J 8:3611–3616
5. Berman N, Maler L (1999) Neural architecture of the electrosensory lateral line lobe: adaptations for coincidence detection, a sensory searchlight and frequency-dependent adaptive filtering. J Exp Biol 202:1243–1253
6. Bertolotto A, Manzardo E, Guglielmone R (1996) Immunohistochemical mapping of perineuronal nets containing chondroitin unsulfated proteoglycan in the rat central nervous system. Cell Tissue Res 283:283–295
7. Borst JG, Helmchen F, Sakmann B (1995) Pre- and postsynaptic whole-cell recordings in the medial nucleus of the trapezoid body of the rat. J Physiol (Lond) 489:825–840
8. Brockhaus J, Deitmer JW (2002) Long-lasting modulation of synaptic input to Purkinje neurons by Bergmann glia stimulation in rat brain slices. J Physiol (Lond) 545:581–593
9. Bruckner G, Brauer K, Hartig W, Wolff JR, Rickmann MJ, Derouiche A, Delpech B, Girard N, Oertel WH, Reichenbach A (1993) Perineuronal nets provide a polyanionic, glia-associated form of microenvironment around certain neurons in many parts of the rat brain. Glia 8:183–200
10. Bruckner G, Bringmann A, Hartig W, Koppe G, Delpech B, Brauer K (1998) Acute and long-lasting changes in extracellular-matrix chondroitin-sulphate proteoglycans induced by injection of chondroitinase ABC in the adult rat brain. Exp Brain Res 121:300–310
11. Bruckner G, Bringmann A, Koppe G, Hartig W, Brauer K (1996) In vivo and in vitro labelling of perineuronal nets in rat brain. Brain Res 720:84–92
12. Bruckner G, Grosche J (2001) Perineuronal nets show intrinsic patterns of extracellular matrix differentiation in organotypic slice cultures. Exp Brain Res 137:83–93
13. Bruckner, G, Seeger G, Brauer K, Hartig W, Kacza J, Bigl V (1994) Cortical areas are revealed by distribution patterns of proteoglycan components and parvalbumin in the Mongolian gerbil and rat. Brain Res 658:67–86
14. Celio MR, Spreafico R, De Biasi S, Vitellaro-Zuccarello L (1998) Perineuronal nets: past and present. Trends Neurosci 21:510–515
15. Colbert CM, Pan E (2002) Ion channel properties underlying axonal action potential initiation in pyramidal neurons. Nat Neurosci 5:533–538
16. Czubayko U, Sultan F, Thier P, Schwarz C (2001) Two types of neurons in the rat cerebellar nuclei as distinguished by membrane potentials and intracellular fillings. J Neurophysiol 85:2017–2029
17. Dodt HU, Zieglgansberger W (1998) Visualization of neuronal form and function in brain slices by infrared videomicroscopy. Histochem J 30:141–152
18. Edwards FA, Konnerth A, Sakmann B, Takahashi T (1989) A thin slice preparation for patch clamp recordings from neurones of the mammalian central nervous system. Pflugers Arch 414:600–612
19. Fernandez FR, Morales E, Rashid AJ, Dunn RJ, Turner RW (2003) Inactivation of Kv3.3 potassium channels in heterologous expression systems. J Biol Chem 278:40890–40898
20. Forsythe ID (1994) Direct patch recording from identified presynaptic terminals mediating glutamatergic EPSCs in the rat CNS, in vitro. J Physiol (Lond) 479:381–387
21. Gabbiani F, Metzner W, Wessel R, Koch C (1996) From stimulus encoding to feature extraction in weakly electric fish. Nature 384:564–567
22. Gähwiler BH (1988) Organotypic cultures of neural tissue. Trends Neurosci 11:484–489
23. Gauck V, Jaeger D (2003) The contribution of NMDA and AMPA conductances to the control of spiking in neurons of the deep cerebellar nuclei. J Neurosci 23:8109–8118
24. Gong B, Rhodes KJ, Bekele-Arcuri Z, Trimmer JS (1999) Type I and type II Na^+ channel alpha-subunit polypeptides exhibit distinct spatial and temporal patterning, and association with auxiliary subunits in rat brain. J Comp Neurol 412:342–352
25. Gray, R, Johnston D (1985) Rectification of single GABA-gated chloride channels in adult hippocampal neurons. J Neurophysiol 54:134–142
26. Hartig W, Derouiche A, Welt K, Brauer K, Grosche J, Mader M, Reichenbach A, Bruckner G (1999) Cortical neurons immunoreactive for the potassium channel Kv3.1b subunit are predominantly surrounded by perineuronal nets presumed as a buffering system for cations. Brain Res 842:15–29
27. Hausen D, Bruckner G, Drlicek M, Hartig W, Brauer K, Bigl V (1996) Pyramidal cells ensheathed by perineuronal nets in human motor and somatosensory cortex. Neuroreport 7:1725–1729
28. Hirono J, Sato T, Tonoike M, Takebayashi M (1992) Simultaneous recording of $[Ca^{2+}]_i$ increases in isolated olfactory receptor neurons retaining their original spatial relationship in intact tissue. J Neurosci Methods 42:185–194
29. Hockfield S (1990) Proteoglycans in neural development. Semin Dev Biol 1
30. Hockfield S, Kalb RG, Zaremba S, Fryer H (1990) Expression of neural proteoglycans correlates with the acquisition of mature neuronal properties in the mammalian brain. Cold Spring Harb Symp Quant Biol 55:505–514
31. Kay AR, Wong RK (1986) Isolation of neurons suitable for patch-clamping from adult mammalian central nervous systems. J Neurosci Methods 16:227–238
32. Koppe G, Bruckner G, Brauer K, Hartig W, Bigl V (1997) Developmental patterns of proteoglycan-containing extracellular matrix in perineuronal nets and neuropil of the postnatal rat brain. Cell Tissue Res 288:33–41
33. Koppe G, Bruckner G, Hartig W, Delpech B, Bigl V (1997) Characterization of proteoglycan-containing perineuronal nets by enzymatic treatments of rat brain sections. Histochem J 29:11–20
34. Kotecha SA, Eley DW, Turner RW (1997) Tissue printed cells from teleost electrosensory and cerebellar structures. J Comp Neurol 386:277–292
35. Kotecha SA, Schlichter LC (1999) A Kv1.5 to Kv1.3 switch in endogenous hippocampal microglia and a role in proliferation. J Neurosci 19:10680–10693
36. Krahe R, Gabbiani F (2004) Burst firing in sensory systems. Nat Rev Neurosci 5:13–23
37. Lafarga M, Berciano MT, Blanco M (1984) The perineuronal net in the fastigial nucleus of the rat cerebellum. A Golgi and quantitative study. Anat Embryol (Berl) 170:79–85
38. Lander C, Zhang H, Hockfield S (1998) Neurons produce a neuronal cell surface-associated chondroitin sulfate proteoglycan. J Neurosci 18:174–183
39. Larkum ME, Kaiser KM, Sakmann B (1999) Calcium electrogenesis in distal apical dendrites of layer 5 pyramidal cells at a critical frequency of back-propagating action potentials. Proc Natl Acad Sci USA 96:14600–14604
40. Lemon N, Turner RW (2000) Conditional spike backpropagation generates burst discharge in a sensory neuron. J Neurophysiol 89:1519–1530
41. Mabuchi M, Murakami S, Taguchi T, Ohtsuka A, Murakami T (2001) Purkinje cells in the adult cat cerebellar cortex possess a perineuronal net of proteoglycans. Arch Histol Cytol 64:203–209
42. Magee JC, Johnston D (1995) Characterization of single voltage-gated Na^+ and Ca^{2+} channels in apical dendrites of rat CA1 pyramidal neurons. J Physiol (Lond) 487:67–90
43. Maler L (1979) The posterior lateral line lobe of certain gymnotoid fish: quantitative light microscopy. J Comp Neurol 183:323–363

44. Maler L, Sas EK, Rogers J (1981) The cytology of the posterior lateral line lobe of high-frequency weakly electric fish (*Gymnotidae*): dendritic differentiation and synaptic specificity in a simple cortex. J Comp Neurol 195:87–139
45. Margrie TW, Brecht M, Sakmann B (2002) In vivo, low-resistance, whole-cell recordings from neurons in the anaesthetized and awake mammalian brain. Pflugers Arch 444:491–498
46. Matthews RT, Kelly GM, Zerillo CA, Gray G, Tiemeyer M, Hockfield S (2002) Aggrecan glycoforms contribute to the molecular heterogeneity of perineuronal nets. J Neurosci 22:7536–7547
47. Milev P, Maurel P, Chiba A, Mevissen M, Popp S, Yamaguchi Y, Margolis RK, Margolis RU (1998) Differential regulation of expression of hyaluronan-binding proteoglycans in developing brain: aggrecan, versican, neurocan, and brevican. Biochem Biophys Res Commun 247:207–212
48. Morris NP, Henderson Z (2000) Perineuronal nets ensheath fast spiking, parvalbumin-immunoreactive neurons in the medial septum/diagonal band complex. Eur J Neurosci 12:828–838
49. Murakami T, Su WD, Ohtsuka A, Abe K, Ninomiya Y (1999) Perineuronal nets of proteoglycans in the adult mouse brain are digested by collagenase. Arch Histol Cytol 62:199–204
50. Noonan L, Doiron B, Laing C, Longtin A, Turner RW (2003) A dynamic dendritic refractory period regulates burst discharge in the electrosensory lobe of weakly electric fish. J Neurosci 23:1524–1534
51. Prescott SA, De Koninck Y (2002) Four cell types with distinctive membrane properties and morphologies in lamina I of the spinal dorsal horn of the adult rat. J Physiol (Lond) 539:817–836
52. Raman IM, Gustafson AE, Padgett D (2000) Ionic currents and spontaneous firing in neurons isolated from the cerebellar nuclei. J Neurosci 20:9004–9016
53. Rashid AJ, Dunn RJ, Turner RW (2001) A prominent soma-dendritic distribution of Kv3.3 K^+ channels in electrosensory and cerebellar neurons. J Comp Neurol 441:234–247
54. Rashid AJ, Morales E, Turner RW, Dunn RW (2001) The contribution of dendritic Kv3 K^+ channels to burst threshold in a sensory neuron. J Neurosci 21:125–135
55. Rose GJ, Fortune ES (1996) New techniques for making whole-cell recordings from CNS neurons in vivo. Neurosci Res 26:89–94
56. Sas E, Maler L (1987) The organization of afferent input to the caudal lobe of the cerebellum of the gymnotid fish *Apteronotus leptorhynchus*. Anat Embryol (Berl) 177:55–79
57. Schoniger S, Wehming S, Gonzalez C, Schobitz K, Rodriguez E, Oksche A, Yulis CR, Nurnberger F (2001) The dispersed cell culture as model for functional studies of the subcommissural organ: preparation and characterization of the culture system. J Neurosci Methods 107:47–61
58. Severson CA, Wang W, Pieribone VA, Dohle CI, Richerson GB (2003) Midbrain serotonergic neurons are central pH chemoreceptors. Nat Neurosci 6:1139–1140
59. Spruston N, Schiller Y, Stuart G, Sakmann B (1995) Activity-dependent action potential invasion and calcium influx into hippocampal CA1 dendrites [see comments]. Science 268:297–300
60. Stoppini L, Buchs PA, Muller D (1991) A simple method for organotypic cultures of nervous tissue. J Neurosci Methods 37:173–182
61. Stuart G, Spruston N, Sakmann B, Hausser M (1997) Action potential initiation and backpropagation in neurons of the mammalian CNS. Trends Neurosci 20:125–131
62. Tanaka M, Maeda N, Noda M, Marunouchi T (2003) A chondroitin sulfate proteoglycan PTPzeta/RPTPbeta regulates the morphogenesis of Purkinje cell dendrites in the developing cerebellum. J Neurosci 23:2804–2814
63. Turner RW, Borg LL, Syed NI (1995) A technique for the primary dissociation of neurons from restricted regions of the vertebrate CNS. J Neurosci Methods 56:57–70
64. Turner RW, Plant JR, Maler L (1996) Oscillatory and burst discharge across electrosensory topographic maps. J Neurophysiol 76:2364–2382
65. Victorov IV, Lyjin AA, Aleksandrova OP (2001) A modified roller method for organotypic brain cultures: free-floating slices of postnatal rat hippocampus. Brain Res Brain Res Protoc 7:30–37
66. Yamaguchi Y (2000) Lecticans: organizers of the brain extracellular matrix. Cell Mol Life Sci 57:276–289